FOPAIR: A Focused Array Imaging Radar for Ocean Remote Sensing

Robert E. McIntosh, *Fellow, IEEE*, Stephen J. Frasier, *Student Member, IEEE,* and James B. Mead, *Member, IEEE*

Abstract—**FOPAIR, a FOcused Phased Array Imaging Radar, provides high-resolution X-band images of the ocean surface. The system is designed to provide high-speed imagery (up to 180 frames/s) for short range applications (50–400 m) from a fixed platform such as a pier or tower. FOPAIR employs a fast, sequentially sampled antenna array and uses a software-based beamforming technique to generate high resolution imagery without the need for multiple radar receivers or beamforming hardware typical of active phased arrays. A summary of the principles of operation and the design of the instrument is given, followed by examples of FOPAIR's imaging capability. To our knowledge, these examples include the highest-resolution, highest-speed microwave images of the ocean surface produced to date. A brief comparison between FOPAIR and synthetic aperture radar techniques is also included.**

I. Introduction

ACHIEVING fine cross-range resolution for imaging in the microwave region requires a physically large radiating aperture. In ground-based applications, this can be implemented by using either a very large antenna with mechanical scanning or by using an array of many smaller antennas with electronic scanning. While mechanically scanned systems are conceptually simpler, phased arrays provide a major advantage due to their ability to scan rapidly and arbitrarily [1].

Conventional antenna arrays are normally designed to resolve targets located in the far-field of the array, and as such are said to be unfocused or "focused to infinity." In the far-field the ratio of target range, R, to array length, D, (or focal ratio, R/D) is typically on the order of 100 or more. For example, the far-field criterion of $R = 2D^2/\lambda$ implies a minimum focal ratio of 100 for a 50λ aperture.

For large aperture and (comparatively) short range applications, the focal ratio is much lower. Focal ratios on the order of ten are not uncommon, and in such cases it is necessary to focus the array into the near-field. Since a near-field focused beam has much the same pattern near the focal point as does it's unfocused counterpart [2], the azimuthal resolution limit of a focused array is simply proportional to $R\lambda/D$ as is the case for unfocused arrays.

A large filled array has many individual elements. If each array element requires dedicated hardware for phase and amplitude control, as is the case for active phased arrays, an expensive hardware design can result. Focusing imposes an additional computational burden on the beamforming signal processor controlling the array adding to the cost and complexity of the system. For certain imaging applications, however, such complexity can be avoided.

For imaging of sufficiently slow-moving scenes, a substantial simplification results by using a sequentially sampled array that time-multiplexes a single radar receiver across many array elements. In this paper, we describe such an imaging system called the FOcused Phased Array Imaging Radar (FOPAIR) which is designed for near-surface ocean remote sensing applications. It consists of a linear array of 128 receive-only antenna elements that share a single radar receiver through a high speed switching network. A separate broad beamwidth transmitter illuminates the radar's field of view. The elements of the receiver array are enabled sequentially on a pulse-by-pulse basis, analogous to the sequential scan of a synthetic aperture radar (SAR). For short to medium range applications a high pulse repetition frequency ensures rapid image capture, and array scans are repeated at up to 180 scans/s. Two-dimensional radar imagery is generated from the unfocused raw data through digital post-processing on a general purpose computer workstation.

The advantages of such a digital beamforming system are many. A single radar transmitter/receiver servicing the entire array substantially reduces system cost. High resolution imagery is acquired from a fixed platform at short to moderate range where each image is captured fast enough to overcome target motion effects, and rapidly repeated scans permit long-term monitoring of a given footprint. Calibration and focusing performed in software permit image data captured once to be processed in many different ways on many resolution scales in azimuth, range, and time.

This paper describes the principles of operation and the design of the FOPAIR sequentially scanned imaging array. It also presents experimental results that show for the first time how such a system can obtain high-resolution images of moving surfaces. Although we refer to well established principles of focused arrays to explain how the system works, we believe that the hardware implementation of this digital beamforming array radar is unique, and that our preliminary experiments demonstrate that high-resolution, high-speed microwave imaging can be accomplished using commercially available data acquisition and signal processing equipment.

In Section II, we review basic principles of focused arrays. In Section III we provide engineering details about the FOPAIR system hardware, and in Section IV we present initial results that demonstrate its performance. We conclude with Section V which outlines the relationship between imagery obtained with FOPAIR and SAR.

Manuscript received November 1, 1993.

The authors are with the Microwave Remote Sensing Laboratory, University of Massachusetts, Amherst, MA 01003 USA.

IEEE Log Number 9406427.

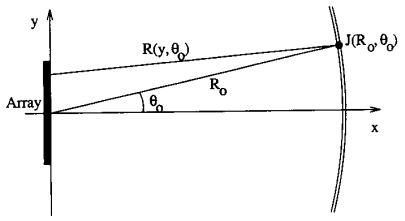

Fig. 1. Focused array geometry.

II. Focused Arrays

Fig. 1 shows a typical geometry for a focused array. Here a broadside array oriented along the y-axis and centered at the origin illuminates the field-of-view including the arc indicated at range R_0. Neglecting range effects on amplitude, the radiated field evaluated along the arc has the form

$$J(R_0,\theta) = \sum_{i=0}^{N-1} E(y_i) e^{-jkR(y_i,\theta)} \tag{1}$$

where $E(y_i)$ is the array aperture field at point y_i and k is the free space wavenumber. The range from the point (R_0,θ) to an arbitrary location along the array is

$$R(y,\theta) = \sqrt{R_0^2 + y^2 - 2R_0 y \sin\theta} \tag{2}$$

which, for $R_0 \gg y$ and for sufficiently small angles (i.e. $\sin\theta \simeq \theta$, $\cos\theta \simeq 1$), can be approximated using

$$R(y,\theta) \simeq R_0 - y\theta + \frac{y^2}{2R_0}. \tag{3}$$

When the y_i are evenly spaced a distance, d, apart (1) becomes

$$J(R_0,\theta) = e^{-jkR_0} \sum_{i=0}^{N-1} E\left(d\left(i-\frac{N}{2}\right)\right) e^{jkd\left(i-\frac{N}{2}\right)\theta} \times e^{-jk\frac{\left(d\left(i-\frac{N}{2}\right)\right)^2}{2R_0}}. \tag{4}$$

By the principle of reciprocity, the array behaves identically in the receiving mode as it does in the transmitting mode. The equation above can therefore be interpreted as the relation between the scattered field received at the aperture, $E(y_i)$, when a distribution of scatterers with reflectivity described by $J(R_0,\theta)$ is illuminated by an external source.

Focusing the array to scan the distribution amounts to computing the sum of (4) for a number of angles. In doing this, the constant phase term outside the sum can be ignored. Additionally, for a given range, the quadratic phase term is identical for all scan angles. Its effect can be removed by including its conjugate in a weighting function, w, applied across the array,

$$w_i = a_i e^{+jk\frac{\left(d\left(i-\frac{N}{2}\right)\right)^2}{2R_0}}. \tag{5}$$

In practice, the weighting function should also include an amplitude taper, a_i, to control array sidelobe levels. After application of the weighting function, the tapered array response

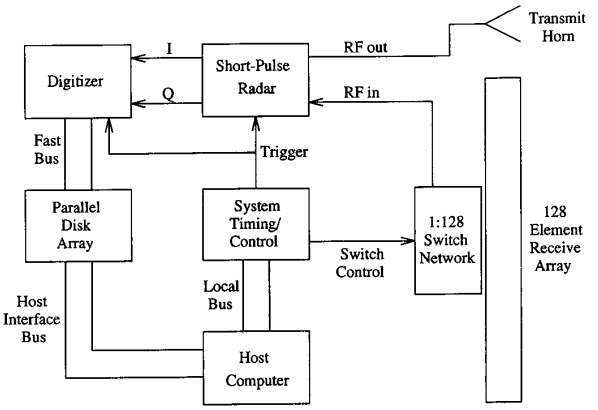

Fig. 2. FOPAIR system block diagram.

and the estimated field distribution are related by a Discrete Fourier Transform relation,

$$J(R_0,\theta) = \sum_{i=0}^{N-1} a_i E\left(d\left(i-\frac{N}{2}\right)\right) e^{jkd\left(i-\frac{N}{2}\right)\theta} \tag{6}$$

as is the case for unfocused arrays operating under far-field conditions [3]. Removing the quadratic phase variation across the array places the focal point of the array at R_0 by transforming the spherical waves reflected by scatterers at that range into plane waves.

A Fast Fourier Transform algorithm can be applied to the responses of the N array elements to yield N evenly spaced samples of the distribution $J(R_0,\theta)$ spanning the visible space of the array. The visible space is determined by the array element spacing according to $-\lambda/2d < \theta < \lambda/2d$. The N samples are separated in angle by λ/Nd which is approximately equal to the beamwidth of the full array.

Having outlined the focusing procedure for one range gate, the measured complex field values from successive range gates can be focused similarly yielding a polar-formatted complex image of the sector illuminated by the transmitter. During processing, the focal point of the array is adjusted as needed to maintain proper focusing at each range gate. Good quality focusing is achieved using this technique provided that the error in the approximation of $R(y,\theta)$ is small compared to a wavelength and provided that worst-case range cell migration effects do not exceed one range gate interval. These conditions are met for practical imaging situations with the instrument.

III. FOPAIR: A Sequentially Scanned Array Imaging Radar

Fig. 2 shows a block diagram of FOPAIR. It consists of an X-Band (10 GHz) short-pulse/pulse-compression radar using a single pyramidal horn to illuminate the entire field-of-view of the radar. The radar receiver is attached to a receiving array through a 1:128 switching network, and a high throughput analog-to-digital converter samples the in-phase and quadrature response of each element. The digitizer

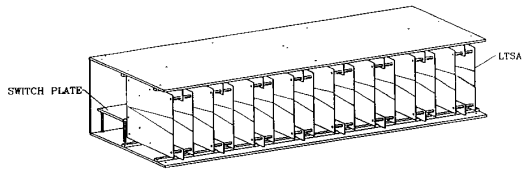

Fig. 3. FOPAIR array module cutout showing 16 LTSA antenna elements.

TABLE I
FOPAIR SYSTEM PARAMETERS

Transmit Antenna	Type	Pyramidal Horn
	Polarization	Vertical
	Azimuth/Elevation Beamwidth	17°
Receive Array	Element Type	Linear Tapered Slot
	Polarization	Vertical
	Azimuth Beamwidth	24°
	Elevation Beamwidth	18°
	Number of Elements	128
	Element Spacing	5.4 cm (1.8λ)
	Array Length	6.8 m
	Array Azimuth Beamwidth	0.25°
	Visible Space	±16°
Radar Transceiver	Peak Power	200 W
	Frequency	10 GHz
	Video Bandwidth	100 MHz
	Effective Pulse Width	10 ns
	Chirp Mode Compression Gain	21.5 dB
Data Acquisition and Storage	Number of Channels	2 (I and Q)
	Sampling Rate	100 MHz
	Quantization	12 bits
	Imaging Capacity	8192 samples/image
	Throughput	160 images/s
	Disk Capacity	2.1 GB

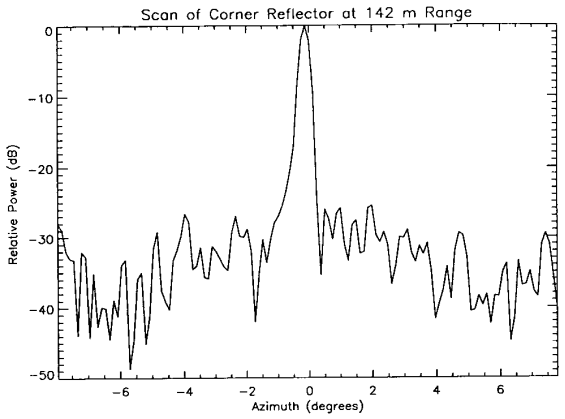

Fig. 4. Azimuth scan of a corner reflector in a grass field at 142-m range. The unfocused signal-to-clutter ratio is approximately 13 dB.

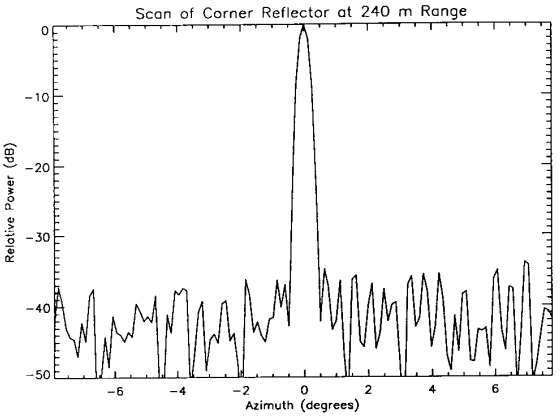

Fig. 5. Azimuth scan of a corner reflector deployed on a boat in calm water at 240-m range. Clutter is negligible, but the unfocused signal-to-noise ratio is approximately 25 dB.

is directly attached to a high speed parallel disk array with a 2.1 gigabyte capacity. An IBM-compatible personal computer controls the entire system.

The receiver array consists of 128 Linear Tapered Slot Antennas (LTSA's) [4]. These are low-cost endfire antennas that are easily fabricated on printed circuit board. The elements are vertically polarized and are fairly directional with 3-dB beamwidths of 18° and 24° in the $E-$ and H-planes respectively. The LTSA's are packaged into modules of sixteen elements placed side by side as shown in Fig. 3. Each module also contains the switching hardware necessary to address each of its elements. The entire array consists of eight such modules deployed end-to-end along a supporting frame.

The 1:128 switching network is implemented in three tiers. The first tier consists of sixteen single-pole-eight-throw (SP8T) switches directly connected to the 128 array elements. The outputs of these switches are connected to a second tier of two SP8T switches that reside in two of the eight antenna modules. Each second tier switch services half of the array and feeds a low noise amplifier (LNA) to establish the noise figure for the receiver. Finally, two long flexible cables connect the LNA outputs to a final single-pole-two-throw (SP2T) switch in the radar receiver.

The radar transmitter/receiver has two operating modes: either a short-pulse mode with 10–100 ns pulses, or a chirp mode where a ten nanosecond pulse is compressed from a two microsecond linear FM chirp. Chirp waveforms are generated in the transmitter and compressed in the receiver using a matched pair of surface acoustic wave dispersive delay lines. The resulting compression gain is approximately 22 dB. A radar image is captured by transmitting and receiving a burst of up to 128 pulses at a pulse repetition frequency of 100 KHz. This provides an unambiguous range of 1500 m and a maximum image capture time of 1.28 ms. The transmitted power in both modes is 200 W (peak) provided by a traveling wave tube amplifier feeding the pyramidal horn illuminator.

The receiver outputs are baseband I and Q channels each with a video bandwidth of up to 100 MHz. These are digitized by a high-throughput sampling system capable of burst mode sampling at rates up to 400 MHz at 12-bits/sample. Typically, the sampler is operated at 100 MHz providing range resolution

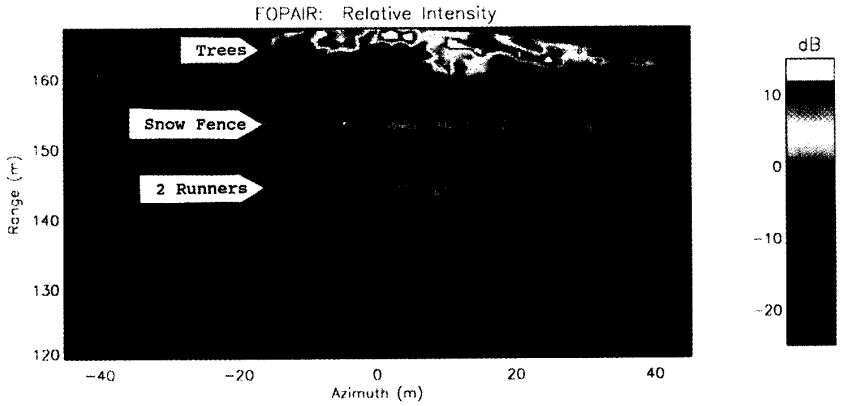

Fig. 6. Backscattered intensity image of an athletic field. Visible features include: trees beyond 160-m range, the vertical posts of a snow-fence at 153-m range, a lacrosse goal at 135-m range (and −2 m azimuth), and two people running at 144-m range.

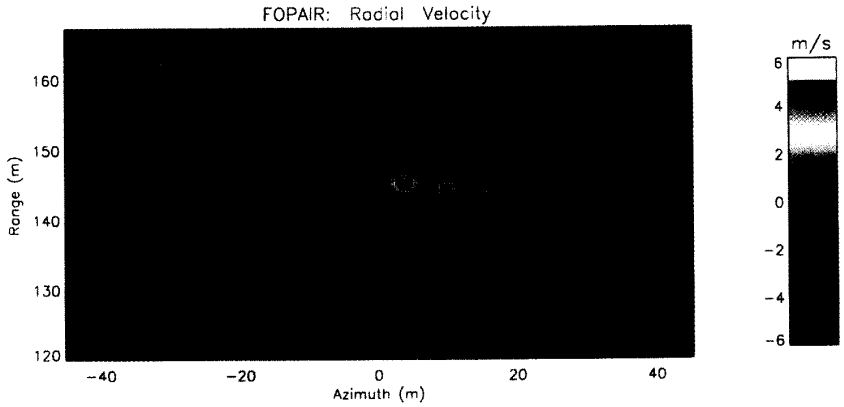

Fig. 7. Radial velocity image corresponding to Fig. 6. Positive velocities are towards the radar. The two runners are clearly visible.

of 1.5 meters. The sampler has an internal capacity of 8192 samples for each of the I and Q channels, so 64 range gates per element may be accommodated if all 128 array elements are used. Alternatively, sub-sections of the array can be used to increase the range depth of the system.

The digitizer stores each burst of captured data on a fast parallel disk-array. The combined throughput of the digitizer and disk-array permits full-resolution imaging at rates up to 160 images/s or half-resolution (using half of the array) imaging at rates up to 180 images/s. The disk array has sufficient capacity to hold approximately 7 min of data captured at the maximum frame rate. The radar, array, and data acquisition systems are all controlled by an IBM-compatible personal computer. The FOPAIR system specifications are outlined in Table I. The array parameters permit scanning within a sector $\pm 16°$ off broadside, although grating lobe rejection constraints limit the practical field of view to within $\pm 12°$. Within this scan limit, worst case range migration effects are no more than one half range cell for practical imaging situations. At a nominal range of 200 meters, an azimuthal footprint of 80 focused pixels spans 70 meters.

The performance of any phased array system depends upon accurate phase and amplitude control of the elements. Due to FOPAIR's modular array design, signals incident on the array elements must travel through varying lengths of cable as they propagate through the switching network. This affects the relative time-of-arrival, phase, and amplitude of the signals received through the array elements, and these must be accounted for to focus the array properly.

Time-of-arrival differences are removed to an accuracy of 2.5 ns by the digitizer. This results in a maximum skew of ± 20 cm in range between corresponding range-gates of adjacent array elements. Phase and amplitude differences are corrected through a field calibration where the array views a point scatterer such as a corner reflector from a moderate distance. Given the range and relative azimuth of the corner reflector, the expected phase and amplitude variation across the array is known and can be used to derive a set of calibration coefficients, one for each element.

The relative sidelobe level (SLL) of the array is determined by the quality of the calibration and upon the phase and amplitude error tolerances of each array element. The quality

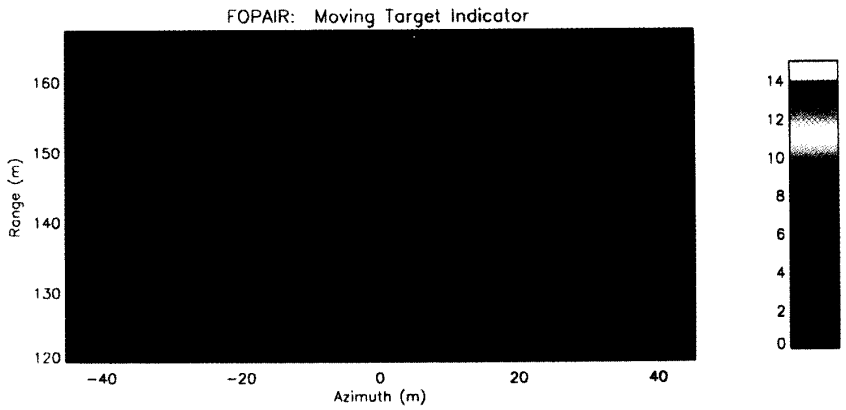

Fig. 8. Moving target indicator (MTI) image corresponding to Fig. 6. The scale is linear. Note the motion of the trees in the background is also visible.

Fig. 9. End-view of the FOPAIR array as mounted on the Scripps Pier. The array is pointed seaward and is tipped down 6° from grazing. The illuminator horn is visible just above the center of the array.

of calibration depends upon how nearly the calibrating scene resembles a point source in free space. Although a corner reflector placed in a field is an adequate calibrating target, the finite signal-to-clutter ratio will give rise to phase and amplitude errors. For example, a point scatterer's reflected signal in the presence of uniform clutter at an (unfocused) signal-to-clutter ratio of 20 dB shows rms phase error of 3° and rms relative amplitude error of ten percent. An approximate analysis of expected SLL's in the presence of random amplitude and phase errors [5] indicates that the average SLL performance is limited to about 35 dB for this signal-to-clutter case.

SLL performance is ultimately limited by mechanical and electrical tolerances in the array itself. Variations in the individual patterns of the LTSA elements indicate that the best average SLL limit is approximately 40 dB. We have achieved relative SLL's of 30 dB in the field with relatively little effort. Figs. 4 and 5 are examples of the performance of such a field calibration.

Fig. 4 shows an azimuth scan of a corner reflector placed in a grass field at range of 142 meters. First the corner reflector was used to generate a set of calibration coefficients, then it was moved and scanned again. The unfocused signal-to-clutter ratio was approximately 13 dB and a 40-dB Chebyshev taper was applied to the array response. The resulting average sidelobes are below 25 dB. The expected average SLL is 29 dB for this case. Fig. 5 shows an azimuth scan of a corner reflector deployed on a boat in calm water at range of 240 m. In this case the clutter fell below the noise floor of the system, so response was signal-to-noise limited with an unfocused signal-to-noise ratio of 25 dB. Again, a 40-dB Chebyshev taper was applied to the array response, and in this case, sidelobes are at least 33 dB below the peak response. The expected average SLL for this case is 37 dB.

IV. Sample Results

Figs. 6–11 show some examples of FOPAIR's imaging capability. The first sequence of images was taken from a field site atop a building on the University of Massachusetts campus where the radar viewed an athletic field adjacent to the building. The array was deployed at a height of 25 m above the field surface, and both the transmitter and the array were tipped down 10° from grazing incidence. These images were acquired using the short-pulse mode of the radar with 10 ns pulses. The frame rate of the radar was 75 Hz.

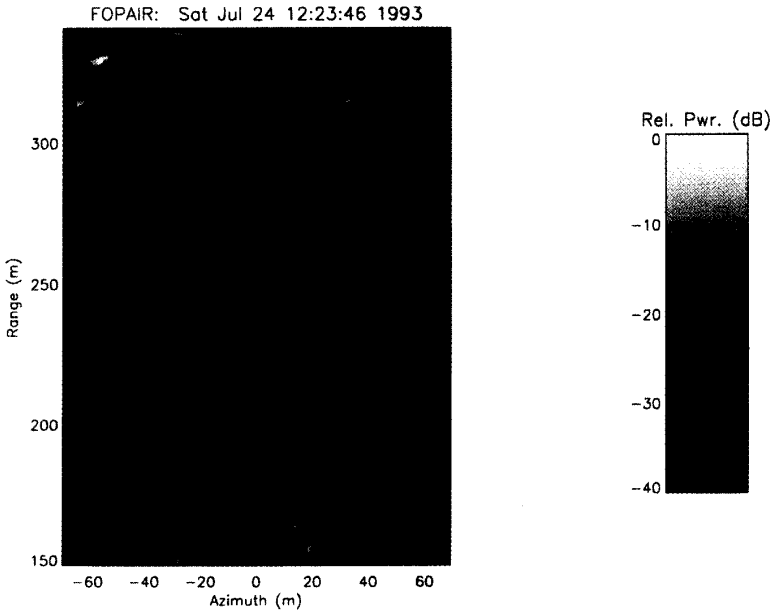

Fig. 10. Backscattered intensity image of ocean waves as viewed from Scripps Pier. Visible structures include a range propagating swell and diagonally propagating wind-waves.

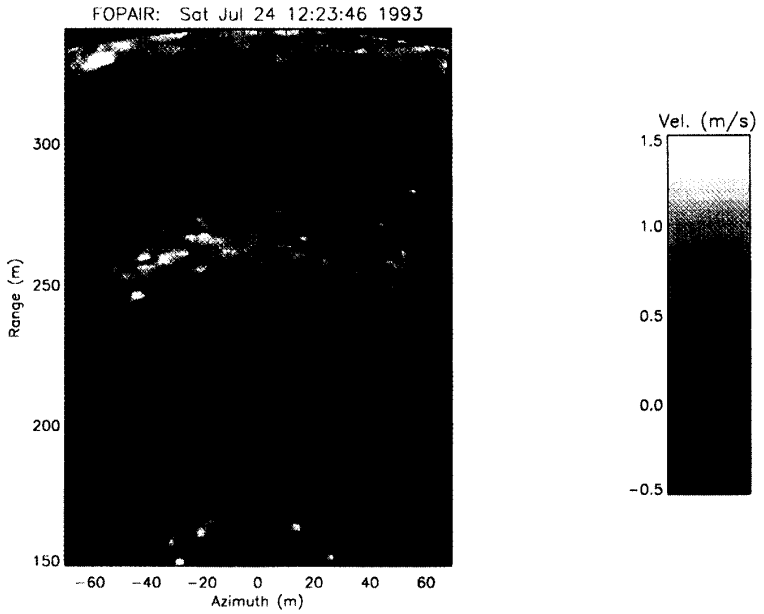

Fig. 11. Doppler velocity image corresponding to Fig. 10. Some pixels have been deliberately set to zero due to low signal-to-noise ratio at those locations.

Fig. 6 shows a backscattered intensity image of the scene. Within the field of view of the instrument were a snow-fence, a lacrosse goal, and two persons running towards the radar. Some trees and a chain link fence occupy the rear portion of the image. The full visible space of the array is displayed, and the effect of the transmitter's antenna pattern is evident in the lower intensities at the scene edges. The grass of the athletic field appears in the blue-to-green intensity levels. The speckled nature of the intensity image is typical of coherent radar imagery. This image was generated using the first field calibration shown in Fig. 4.

When a sequence of complex images are captured, radial velocity and moving-target-indicator (MTI) images can be generated to discriminate between moving and stationary

targets. Radial velocity images are derived using the covariance or "pulse-pair" technique [6] which approximates velocity from the frame-to-frame phase difference of each complex image. MTI images are derived from frame-to-frame differences in intensity. Fig. 7 shows a radial velocity image corresponding to the backscattered intensity image of Fig. 6. The maximum unambiguous velocity was increased beyond the limit imposed by the 75 Hz frame rate by processing two successive scans of half the array. Fig. 8 shows an MTI image of the scene.

During July 1993, FOPAIR was deployed on the research pier at the Scripps Institute of Oceanography in La Jolla, CA, where initial ocean measurements were conducted over a three week period. A photo of the array's installation is shown in Fig. 9 where the array looks seaward from a height of 12 m. Figs. 10 and 11 are backscattered intensity (corrected for range and antenna pattern effects) and Doppler velocity images respectively of the ocean surface as viewed by FOPAIR. The sector shown in the images spans $\pm 12°$. For these images 64 antenna elements were used, allowing 128 range gates and an image depth of nearly 200 m. The frame rate of the radar was 180 Hz.

Two major wave structures are visible in both images. One is a swell which propagates normally towards the shore (and the radar) with a wavelength of about 80 m. The other structure is a wind-generated wave train that propagates diagonally from the upper left to the lower right of the image. The significant wave height during this measurement was 50 cm, and winds were approximately 5 m/s nearly aligned with the wind-wave propagation direction. The wavelength of the large scale swell is easiest to determine from the Doppler velocity image, whose contrast (for this imaging geometry) is determined by variation in the horizontal component of the long-wave orbital velocity. The smaller scale wind-waves are more obvious in the backscattered intensity image. These images are averaged results from 18 complex images acquired over a 0.1 s period. Because only 64 array elements were used, these images represent half of FOPAIR's azimuthal resolution capability.

V. Analogy to SAR

Although FOPAIR is designed for imaging areas much smaller in scale than in most SAR applications, it does share SAR's sequentially sampled array approach. It is worthwhile, therefore, to consider the relationship between FOPAIR imagery and side-looking SAR imagery.

Airborne SAR is a focused array system that uses the azimuthal translation of a single radar antenna to synthesize an aperture whose size is limited principally by the antenna's footprint. Because the antenna's footprint increases linearly with range and because the antenna traverses multiple synthetic aperture intervals, the focused side-looking SAR resolution limit is range and wavelength independent and equal to half the radar antenna's real aperture dimension [7]. Since FOPAIR is stationary, only one array aperture is available for processing, and as a result, FOPAIR's azimuthal resolution

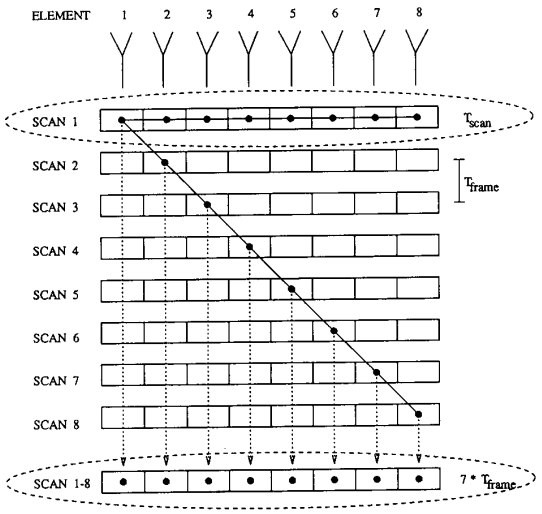

Fig. 12. Diagram depicting time-delayed aperture synthesis using a full resolution data set. The example shown is for an 8-element array.

limit is both range dependent and limited by the physical extent of the array.

A side-looking SAR achieves its resolution limit by match-filtering the unfocused raw data with a kernel representing the signature of a broadside target at a given range (this kernel is essentially the same quadratic phase function used for the focus correction in FOPAIR's processing). Thus, the side-looking SAR focusing algorithm implements one broadside beam operating in a pushbroom-mode moving at the rate of the airborne platform. Many overlapping synthetic apertures are used to generate Cartesian-formatted strip-map imagery. Since FOPAIR has only a single aperture available, it must implement multiple beams over a range of look angles to achieve azimuthal spatial coverage. The resulting imagery is polar-formatted.

For side looking airborne SAR's, aperture synthesis intervals are of the order of one second [8]. This long coherent integration time can be troublesome when viewing a target such as the ocean where decorrelation times can be measured in tens of milliseconds [9]. As a result, SAR images of the ocean necessarily contain data retrieved over several decorrelation times. The effect of decorrelation (and surface motion) within the aperture synthesis time has been the subject of considerable research interest in interpretation of SAR imagery of ocean waves [8], [10], [11]. Since FOPAIR can scan rapidly, on the order of 1 millisecond, the effect of such decorrelation is mitigated and high-resolution images are acquired essentially instantaneously.

By increasing the aperture synthesis time of the FOPAIR array, the effects of ocean surface motion on SAR image formation can, to some extent, be explored. We illustrate how this might be done using a single data set by comparing images formed using an aperture synthesized over several array scans with images formed using a single scan. For example, combining the responses of array element 1 from scan 1, element 2 from scan 2, element 3 from scan 3,

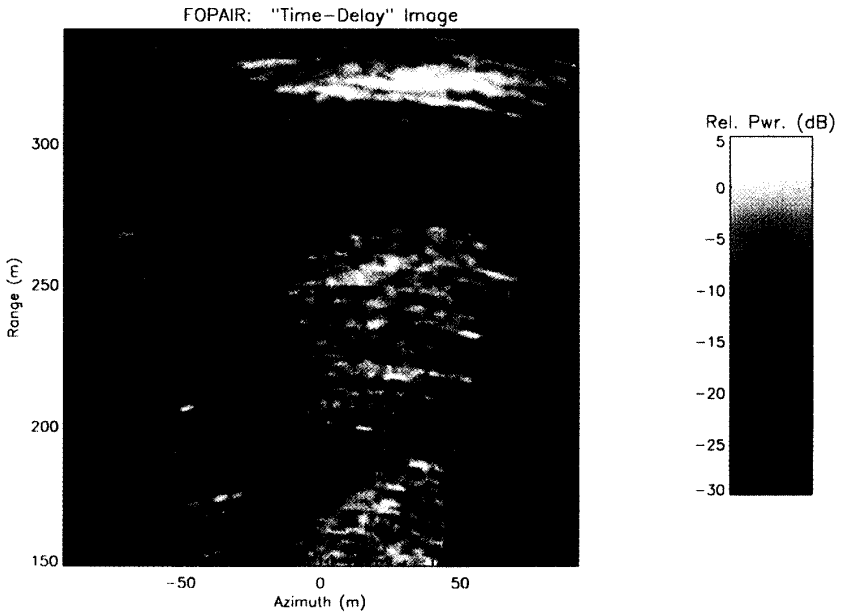

Fig. 13. Average of 16 overlapped time-delay processed images of ocean waves showing displacement of image features to the right and azimuthal smearing. Some features in the image have aliased to the left side of the array's visible space. The coherent integration time for each of the 16 images comprising this average is 350 ms.

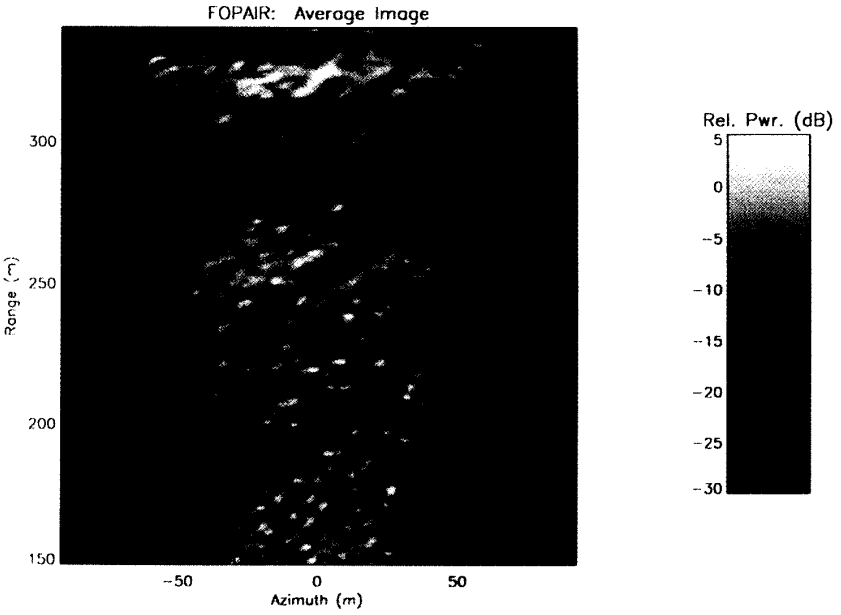

Fig. 14. Average of 80 normally processed images spanning the same total time period used to form Fig. 13. The coherent integration time for each of the 80 images comprising the average is 0.64 ms.

etc., results in a "time-delayed" synthesized aperture with a much longer integration period. The sampling scheme shown in Fig. 12 illustrates this concept.

Figs. 13 and 14 show a comparison of such time-delay processed imagery with normally processed imagery. Fig. 13 is the incoherent average of 16 backscattered intensity images, each synthesized using 64 array elements distributed over 64 array scans. Thus each image had a 350 ms coherent integration time. The 16 individual images comprising the average were displaced slightly in time (i.e. image 1 from

scans 1–64, image 2 from scans 2–65, etc.) so that the total time period represented by this averaged image is 80 array scans or 440 ms. The time averaging reduces the effects of speckle permitting a reasonable comparison with Fig. 14, an incoherent average of 80 normally generated intensity images from the same 80 array scans. These images show the entire visible space of the array without correction for the transmitter's antenna pattern to permit easier comparison of major image features.

The most obvious difference between Fig. 13 relative to Fig. 14 is the azimuthal displacement of image features to the right and the reduction in azimuthal resolution. We attribute the overall displacement effect to the mean sensed radial velocity of scattering facets in the scene during the long aperture synthesis time of the array. It is the same displacement observed in SAR imagery of moving targets and is not a squinting of either the illuminating or receiving antenna patterns. The degree of squint can be predicted by considering the progressive phase response across the array due to a scatterer moving at a constant radial velocity. In addition to the scatterer's normal signature (a quadratic phase variation across the focused array), an additional linear phase variation results from its radial motion. The incremental linear phase shift between adjacent array elements is equal to $2k\Delta r = 2kv_r\Delta t$, where Δr is the change in range of a scatterer moving at radial velocity, v_r, in the time interval, Δt, and k is the free-space wavenumber. Equating the incremental phase shift to that expected from a stationary scatterer located off-broadside yields

$$2kv_r\Delta t = kd\sin(\Delta\theta) \tag{7}$$

where d is the array element spacing. Solving for the resulting apparent squint, $\Delta\theta$, yields

$$\Delta\theta = \sin^{-1}\left(\frac{2v_r\Delta t}{d}\right) \simeq \frac{2v_r\Delta t}{d}. \tag{8}$$

The array element spacing is 5.4 cm, and the time interval between array scans is 5.56 ms. Fig. 11 indicates that typical measured radial velocities are on the order of 0.5 m/s. This area average velocity includes contributions both from surface drift current and from the phase velocity of Bragg-resonant ripples responsible for the bulk of the backscattered microwave signal [12]. The ripples are 1.5 cm in wavelength and travel at a phase velocity of about 0.25 m/s. As the radar is looking generally upwind, this phase velocity can account for about half of the measured mean velocity.

Combining these values yields an expected average squint of $+6°$, which is consistent with the squint angle observed in Fig. 13. Note that the actual squint angle should vary somewhat in range due to the orbital velocity of the long waves modulating the sensed radial velocity, although it is not obvious in the figure. The azimuthal smearing is due to a number of mechanisms including the spatial variation of displacements due to long-wave orbital motion and defocusing due to orbital accelerations [11], as well as smearing due to rapid decorrelation of localized features [13].

VI. Summary

FOPAIR, a unique implementation of a focused array imaging radar, has been described, and its performance has been illustrated with sample images of scenes containing both stationary and moving scatterers. While the ocean imaging results presented here are preliminary, they do indicate that FOPAIR is capable of high-resolution coherent imaging of small to medium scale wave features with excellent spatial resolution and little or no degradation due to the finite aperture synthesis time. Furthermore, by degrading the effective aperture synthesis time, the adverse effects of surface motion on synthetic aperture imagery are revealed.

Acknowledgment

The authors wish to acknowledge S. Targonski and Professor D. Pozar of the UMASS Antenna Laboratory and P. Langlois of Quadrant Engineering, Inc. for their assistance in the design and fabrication of the LTSA elements and of the FOPAIR array. Recognition is also due to Drs. R. K. Moore, R. Beal, G. Brown, W. J. Plant, D. R. Lyzenga, F. Herr, and C. T. Swift, who participated in initial discussions regarding the development of FOPAIR.

References

[1] B. D. Steinberg, *Principles of Aperture and Array System Design.* New York: Wiley, 1976.
[2] J. W. Sherman, "Properties of focused apertures in the Fresnel region," *IRE Trans. Ant. Propagat.*, vol. AP-10, pp. 399–408, 1962.
[3] D. L. Mensa, *High Resolution Radar Cross Section Imaging.* Dedham, MA: Artech House, 1991.
[4] K. S. Yngvesson, D. H. Schaubert, T. L. Korzeniowski, E. K. Kollberg, T. Thorngren, and J. F. Johansson, "Endfire tapered slot antennas on dielectric substrates," *IEEE Trans. Ant. Propagat.*, vol. AP-33, pp. 1392–1400, 1985.
[5] R. S. Elliot, "Random errors in uniformly spaced arrays," in R. C. Hansen, ed.,*Microwave Scanning Antennas*, vol. 2. Port Angeles, WA: Peninsula, 1985, ch. 1.
[6] K. S. Miller and M. M. Rochwarger, "A covariance approach to spectral moment estimation," *IEEE Trans. Informat. Theory*, vol. IT-18, pp. 588–596, 1972.
[7] F. T. Ulaby, R. K. Moore, and A. K. Fung, *Microwave Remote Sensing: Active and Passive*, vol. 2. Dedham, MA: Artech House, 1982.
[8] W. R. Alpers, D. B. Ross, and C. L. Rufenach, "On the detectability of ocean surface waves by real and synthetic aperture radar," *J. Geophys. Res.*, vol. 86, no. C7, pp. 6481–6498, 1981.
[9] B. L. Lewis and I. D. Olin, "Experimental study and theoretical model of high resolution radar backscatter from the sea," *Radio Sci.*, vol. 15, no. 4, pp. 815–828, 1980.
[10] C. T. Swift and L. R. Wilson, "Synthetic aperture radar imaging of moving ocean waves," *IEEE Trans. Ant. Propagat.*, vol. AP-27, pp. 725–729, 1979.
[11] K. Hasselmann, R. K. Raney, W. J. Plant, W. Alpers, R. A. Shuchman, D. R. Lyzenga, C. L. Rufenach, and M. J. Tucker, "Theory of synthetic aperture radar ocean imaging: A MARSEN view," *J. Geophys. Res.*, vol. 90, no. C3, pp. 4659–4686, 1985.
[12] J. W. Wright, "A new model for sea clutter," *IEEE Trans. Antenna Propagat.*, vol. AP-16, pp. 217–223, 1968.
[13] D. R. Lyzenga and R. A. Shuchman, "Analysis of scatterer motion effects in MARSEN X-band SAR imagery," *J. Geophys. Res.*, vol. 88, no. C14, pp. 9769–9775, 1983.

Robert E. McIntosh (S'66–M'67–SM'72–F'85) received the B.S. degree from Worcester Polytechnic Institute, Worcester, MA, in electrical engineering in 1962, the M.S. degree from Harvard University, Cambridge, MA, in 1964, and the Ph.D. degree from the University of Iowa, Iowa City, in 1967.

He was a Member of the Technical Staff of Bell Telephone Laboratories, Inc., in North Andover, MA, from 1962 until 1965, where he worked in a microwave networks group. In 1967, he joined the Department of Electrical and Computer Engineering at the University of Massachusetts, where he is now a Professor. He spent the 1973–1974 academic year as Guest Professor of Experimental Physics at the University of Nijmegen in the Netherlands, and 1980–1981 with the Electromagnetics Research Branch at NASA Langley Research Center. He served as coordinator of the Microwave Electronics Group from 1981 until 1987, and now codirects the Microwave Remote Sensing Laboratory. His teaching and research interests are in electromagnetic field theory, microwave engineering, wave propagation, and remote sensing.

Dr. McIntosh received the Senior Faculty Scholarship Award from the College of Engineering Alumni in 1984, the General Electric Teaching Award in 1988, and ECE Department HKN Teaching Awards in 1987 and 1990. In 1992, he was selected as a speaker for the University of Massachusetts distinguished faculty lecture series. He is a recipient of the IEEE Centennial Medal. He served on the Administrative Committees of the Geoscience and Remote Sensing Society and the Antennas and Propagation Society, and was elected president of the GRS-S in 1984 and AP-S in 1985. He received the GRS-S Distinguished Service Award in 1985. He has been member of the United States National Committee of URSI since 1984. He served as an associate editor and as editor-in-chief of the IEEE TRANSACTIONS ON ANTENNAS AND PROPAGATION. He was also an associate editor of *Radio Science*, a guest editor for special issues of the IEEE TRANSACTIONS ON GEOSCIENCE AND REMOTE SENSING and for the IEEE TRANSACTIONS ON EDUCATION. He was the general chairman of the 1976 International AP-S/URSI Symposium and the 1985 International Geoscience and Remote Sensing Symposium held in Amherst and was the Technical Program Chairman for the 1990 URSI Commission F International Symposium on Microwave Signatures in Remote Sensing in Hyannis, MA. As a member of the Technical Activities Board of the IEEE and Commissions B, C, F, and H of the USNC/URSI, he has served on numerous technical subcommittees. He also consults for industry and various governmental agencies and has participated in numerous NSF, DoD, NASA, and NAS panels and workshops. He cofounded Quadrant Engineering, Inc. in 1982. He is a member of the American Physical Society, the American Geophysical Union, Sigma Xi, Tau Beta Pi, Phi Kappa Phi, and Eta Kappa Nu.

Stephen J. Frasier (S'94) received the B.S.E.E. degree from the University of Delaware in 1987. He is currently pursuing a Ph.D. in electrical and computer engineering at the Microwave Remote Sensing Laboratory (MIRSL) at the University of Massachusetts, Amherst.

From 1987 to 1990, he worked at SciTec, Inc. (now a subsidiary of TRW) in Princeton, NJ, where he was primarily involved in digital signal and image processing applications. At MIRSL he has led the development of the FOPAIR radar's RF, data acquisition/control, and imaging software subsystems.

Mr. Frasier is a student member of Tau Beta Pi and Eta Kappa Nu.

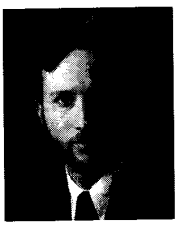

James B. Mead (S'86–M'89) received the B.S.E.E. degree from the University of Virginia, Charlottesville, in 1981, and the Ph.D. degree in electrical and computer engineering from the University of Massachusetts, Amherst, in December 1989.

Since December 1989, he has been a Senior Research Fellow at the University of Massachusetts Microwave Remote Sensing Laboratory. There, he is involved in the conception, design, fabrication and test of microwave and millimeter wavelength instrumentation. His research includes millimeter-wave cloud studies, polarimeter studies of snow cover and vegetation, ocean surface scattering, and turbulence imaging. His is currently responsible for the development of the Turbulent Eddy Profiler, sponsored by ARO. Since March 1990, he has also been a Senior Research Engineer at Quadrant Engineering, Amherst, MA. There, he is a Principal Investigator of the Focused Phased Array Imaging Radar (FOPAIR) program supported by the U.S. Navy, and is in charge of all aspects of system design, fabrication, and testing. He was also a Senior Scientist for an NSF-funded ocean-based boundary layer wind profiler development, principal investigator of an NOAA-funded SBIR to develop radar for hurricane reconnaissance aircraft for measuring ocean wind speed and direction, and Principal Investigator of a Navy-funded SBIR to develop a Turbulent Eddy Profiler for ship-based operations.